The thin border between cloud and aerosol: sensitivity of several ground based observation techniques.

Josep Calbó[a,*], Charles N. Long[b,c], Josep-Abel González[a], John Augustine[c], Allison McComiskey[c]

[a] Departament de Física, Universitat de Girona, Girona, Spain

[b] Cooperative Institute for Research in the Environmental Sciences, University of Colorado Boulder, Co, USA

[c] National Oceanic and Atmospheric Administration, Earth System Research Laboratory, Global Monitoring Division, Boulder, Co, USA

* Corresponding author

Abstract

Cloud and aerosol are two manifestations of what it is essentially the same physical phenomenon: a suspension of particles in the air. The differences between the two come from the different composition (e.g., much higher amount of condensed water in particles constituting a cloud) and/or particle size, and also from the different number of such particles (10-10,000 particles per cubic centimeter depending on conditions). However, there exist situations in which the distinction is far from obvious, and even when broken or scattered clouds are present in the sky, the borders between cloud/not cloud are not always well defined, a transition area that has been coined as the "twilight zone". The current paper presents a discussion on the definition of cloud and aerosol, the need for distinguishing or for considering the continuum between the two, and suggests a quantification of the importance and frequency of such ambiguous situations, founded on several ground-based observing techniques. Specifically, sensitivity analyses are applied on sky camera images and broadband and spectral radiometric measurements taken at Girona (Spain) and Boulder (Co, USA). Results indicate that, at these sites, in more than 5% of the daytime hours the sky may be considered cloudless (but containing aerosols) or cloudy (with some kind of optically thin clouds) depending on the observing system and the thresholds applied. Similarly, at least 10% of the time the extension of scattered or broken clouds into clear areas is problematic to establish, and depends on where the limit is put between cloud and aerosol. These findings are relevant to both technical approaches for cloud screening and sky cover categorization algorithms and radiative transfer studies, given the different effect of clouds and aerosols (and the different treatment in models) on the Earth's radiation balance.

1. Introduction

The Earth's atmosphere contains suspended particles, i.e. particles that because of their size have terminal fall velocities of the order of centimeters per second at most, so they have atmospheric residence times on the order of hours, days, or much longer in some cases. These particles vary in their chemical composition, have concentrations that vary in space and time, are present in both the solid and liquid phases and have sizes ranging over several orders of magnitude. In gross aggregate, the suspension of particles receives two names: either cloud or aerosol. Simplifying, a cloud is an aggregate of a number of particles formed mainly of water, in liquid or solid state (i.e., hydrometeors) of sizes between a few microns to some millimeters and in sufficient concentration to be perceived by human vision from the Earth's surface. Any other aggregate of particles is called, generically, atmospheric aerosol, and generally contains less liquid water than clouds. This includes wind-borne dust, sea spray particles of salt, sulfate and organic particles, or ash and soot arising from combustion. Precipitating particles such as rain, snow or hail (which have terminal fall velocity of the order of meters per second) are excluded from this discussion.

Despite the above differences in origin and composition, clouds and aerosol could be considered two manifestations of the same phenomenon. However, their description, characteristics, and –in particular− interactions with solar and terrestrial radiation have historically been studied separately. Indeed, the study of clouds extends back to ancient times whereas the study of atmospheric aerosol is much more recent. In fact, the term was proposed in the early 20th century, and has become popular within the atmospherics science community only after the 1960s or so, as previously unspecific names (dust, smoke, etc.) or more technical designations (lithometeor, etc.) were used. The interactions between clouds and aerosols are known, although their climatic significance is far from being fully quantified (see the reviews of Heintzenberg 2012; Rosenfeld et al. 2014; Seinfeld et al. 2016). The presence of different types or concentrations of aerosols has impacts on clouds, as some particulate matter (cloud condensation nuclei or ice nuclei) are more amenable for water vapor to condense into droplets or crystals to form clouds. These effects, especially in the field of energy balance, have been known as aerosol indirect effects (Albrecht, 1989; Twomey, 1974) to distinguish from the direct (purely radiative by absorption and scattering) effect that aerosols have on the radiative energy transfer in the atmosphere.

Broadly speaking, there are two features that distinguish a cloud from other suspension of particles in the air: i) the content of water in droplets and/or ice crystals, and ii) the visibility, i.e., the appearance of a more or less clearly delimited form of (usually) white/grey color, which is possible to see evolve (it should be noted that some aerosol suspensions are also clearly visible, for example, a smoke plume). Both features allow quantification, i.e. one can propose a threshold for the concentration of droplets or ice crystals (or for the amount of condensed water), and also for the optical effect (the optical thickness at a certain wavelength). Dupont et al. (2008) showed that solar irradiance and sky imagery retrievals tuned to reflect human observations allow up to a visible optical depth of 0.15 to 0.2 of primarily high ice haze to be traditionally classified as “cloud free” sky. But historically the decision on whether a volume of air is cloud or not (leaving no room for intermediate cases) has been based on the judgment of a human observer on the ground. This does not seem very scientific, since it can happen that the same volume of air containing aqueous particles are labeled as cloud or not depending on the contextual conditions in which the observation is made, subject to the judgment and perception of the observer. Similar difficulties arise when clouds are observed from satellites (Koren et al., 2008).

Consequently, fundamental questions remain: What is the limit of visibility from which a suspension of droplets must be considered cloud? Should this limit be set for an "average" human eye, or can it be objectively established for some instrument as in Dupont et al. (2008)? Or is it even reasonable to consider such a limit given that the aerosol/cloud particle suspension could be considered as a continuum and not a dichotomic phenomenon. How does one define visibility when observations are performed in a wavelength outside the visible range of the human eye? Droplets form on soluble hydrophilic particles whereas many ice particles form on insoluble hydrophobic particles so how does one decide if the suspended particles are aerosol particles or hydrometeors? When observation is performed by automated instruments, trying to reduce to a three level classification (cloud / aerosol / clear sky) is even more difficult (Tapakis and Charalambides, 2013). Subsequently, this classification has consequences for climate studies (Charlson et al., 2007), including trend analysis, as derived trends may depend on the instrument and/or methodology used to infer cloud amounts (Wu et al., 2014).

A good example of the difficulties of defining cloud and aerosol is found regarding sky images taken by "all-sky" cameras (they "see" an entire 180° sky view from a particular point at the surface). The digital images are analyzed to obtain information on the state of the sky, in particular cloud cover and cloud type (Calbó and Sabburg, 2008; Heinle et al., 2010; Kazantzidis et al., 2012; Long et al., 2006b). The problem is what thresholds to set to distinguish between the "clear" and "cloudy" pixels. Even if more complex approaches are adopted (Li et al., 2011; Saito and Iwabuchi, 2016), they rely on the initial human decision taken on the training images. In fact, sky cameras have also been proposed as devices to observe and characterize the atmospheric aerosol (Cazorla et al., 2008).

This is not unique for cloud observations by ground-based imaging in the visible. For example, the difficulties in trying to distinguish clouds and aerosol in sunshine duration records have been pointed out elsewhere (Sanchez-Romero et al., 2014). In addition, many works focus on removing cloud "contamination" from aerosol observations performed with sunphotometers or shadowband radiometers (Alexandrov et al., 2004; Kassianov et al., 2013; Michalsky et al., 2010). The problem further expands when considering other views (satellite) or other wavelengths (ceilometers in the infrared, microwave radiometers, weather radars). All these difficulties have consequences in both meteorological and climatological studies (e.g. Boers et al., 2010; Várnai and Marshak, 2011; Sanchez-Lorenzo et al., 2009; Wu et al., 2014).

In general the distinction between a cloudy and a cloudless sky, and the separation between cloud and aerosol, is appropriate for attribution studies and modeling radiative effects of different climate forcing mechanisms, but imposing this classification may be unnecessary (or inconvenient) in relation to new and advanced methods of observation and measurement. If so, the distinction could also be unnecessary in radiative transfer models, or in future parameterizations included in weather and climate models. This approach of a continuous treatment of aggregates of particles in the atmosphere is relatively new, although some previous works have already pointed in this direction.

For example, Charlson et al. (2007) highlighted the importance that has been given to the separation between the "cloud" and "clear" regimes in various fields of study including the radiative forcing by clouds and the quantification of direct effects and indirect radiative forcing by aerosols. The paper questioned the separation between the two regimes, and suggested the desirability of treating the phenomenon as a continuum. Similarly, Koren et al. (2007) described a transition zone ("twilight" zone) around the cloud in which the optical properties are close to those of the cloud itself. The authors estimated that an appreciable fraction (between 30 and 60%) of the part of the globe at any given time considered free of clouds could correspond to that area of transition, a fact that could have important climate implications. The question of the climatic importance of clouds that are considered "small" in size was addressed by Koren et al. (2008), as well as the effect of the aerosol in the regions between clouds (Koren et al., 2009). Also, Bar-Or et al. (2010) introduced the concept of cloud field as an area that includes detectable clouds and twilight zone, and found that the cloud field fraction could be as large as 97% in an area where the detectable cloud fraction is 53%. In the cited works, several methodologies were used: spectral radiometry from the surface in the visible and near infrared, satellite measurements, and modeling. Also long-wave spectral radiometry is being used for the purpose of studying the properties of thin clouds and the transition region (Hirsch et al., 2014, 2012).

Other researchers have studied radiative effects occurring in the vicinity of the clouds. Thus, the question of increased reflectivity and the "bluish" aerosol in the vicinity of the visible clouds has been attributed to the Rayleigh scattering of the radiation reflected by the cloud; that is ultimately a three-dimensional effect (Eck et al., 2014; Kassianov et al., 2010; Marshak et al., 2008; Várnai and Marshak, 2009; Wen et al., 2008). They have also studied the transition region from satellite measurements and stated its important radiative effects (Várnai and Marshak, 2011) and have explored the combination of data from two different satellites with the goal of obtaining detailed information on aerosols near clouds (Várnai and Marshak, 2012). Recently, Ten Hoeve and Augustine (2016) confirmed from ground-based and satellite measurements that the aerosol optical depth increases in the vicinity of a cloud; Jeong and Li (2010) had previously found that aerosol humidification effects could explain one fourth of a reported correlation between cloud cover and aerosol optical depth. Moreover, Chiu et al. (2009) and Marshak et al. (2009) addressed the description of the continuum from measurements of zenith spectral radiance in the visible and near infrared, with the high temporal resolution that the rapid transitions between cloud and clear sky require. Chiu et al. (2010) successfully replicated these results by radiative modeling.

The goal of the current paper is to quantify the importance and frequency of situations where ambiguity between clouds and aerosol occur; in other words, situations where the suspension of particles depend on subjective definition to be classified as either cloud or aerosol. These transition situations populate the continuum between what is clearly a cloud and what is to be called undoubtedly an aerosol. We realize that such quantification depends both on the instrument or technique used for observing the sky, and on the climate and geographical conditions of the site. Therefore, several ground-based, passive observing techniques are considered: specifically, sensitivity analyses are applied on sky camera images, broadband radiation measurements, and spectral measurements. Two sites are considered: Girona (Spain), and Boulder (Co, USA).

2. Data, measurements, and observations

The University of Girona has maintained a radiometric and meteorological station since the early 1990s. Instruments are placed on the roof of a university building (41°58′N, 2°50′E, 110 m asl). The site is located in the northeast of the Iberian Peninsula, some 30 km from the Mediterranean Sea and 40 km from the Pyrenees mountain range; the climate is Mediterranean, meaning mild winters and hot summers, and relatively dry, with more rain in equinoctial seasons. Characteristics of the site and of instruments of this station can be found in Calbó et al. (2016); here we will only give some details of the relevant instruments used in the current research. First, the site holds a set of instruments measuring downwelling shortwave (solar) and longwave (atmospheric) radiation, including the three components for the solar irradiance (global, direct, and diffuse). These instruments strive to adhere to the specifications of the Baseline Surface Radiation Network (BSRN) for calibration, daily routine supervision, and temporal resolution of sampling and recording data. Second, operation of a Multifilter Rotating Shadowband Radiometer (MFRSR) began at the site in 2012. This instrument is oriented towards characterizing the atmospheric aerosol, specifically its optical depth (AOD) at several visible and near infrared wavelengths and is described elsewhere (Harrison et al., 1994; Sanchez-Romero et al., 2016). The MFRSR measures both global and diffuse solar radiation in one broadband and six narrow bands of the solar spectrum (specifically the narrow band filters are centered nominally at 400, 500, 615, 670, 870, and 940 nm). The MFRSR at Girona sampled at 1 minute time step until September 2014; since October 2014 it has sampled at 15 second intervals. Third, a whole sky camera is used to take images of the sky during daylight hours, at 1 minute time steps. The camera is a conventional digital CCD camera, provided with a fish-eye (i.e. >180º field-of-view) lens and mounted on a sun tracker, in such a way that a black sphere projects its shadow on the lens, blocking the direct sun from entering the camera. In the current research, one year (2014) of data and observations from each of these instruments will be analyzed.

The Surface Radiation Budget Network (SURFRAD) was established in 1993 through the support of the National Oceanic and Atmospheric Administration (NOAA) Office of Global Programs. Its primary objective is to support climate research with accurate, continuous, long-term measurements of the surface radiation budget over the United States. Thus, currently seven SURFRAD stations are operating across the US (Augustine et al., 2005, 2000). Here we will use data and observations from one site, which is the NOAA-Earth System Research Laboratory Test Facility at Table Mountain, located 13 km north of Boulder (40º7'N, 105º14'W, 1689 m asl). The instruments used here are part of a larger set maintained at this location and used for annual intercomparisons and other research. Radiation measurements at SURFRAD stations cover the range of the electromagnetic spectrum that affects the earth/atmosphere system. Like in Girona, total downwelling (global) solar radiation is measured by an upward looking broadband pyranometer, the direct component is monitored with a normal incidence pyrheliometer mounted on an automatic sun tracker, the diffuse component is measured by a shaded pyranometer that rides on the same tracker, and an upward looking pyrgeometer measures longwave (thermal infrared) radiation emitted downward by clouds and other atmospheric constituents. In addition, a third pyranometer and another pyrgeometer are mounted facing downward, on cross arms atop of a 10-meter tower to measure solar radiation reflected from the surface and upwelling long wave radiation respectively. Similar to Girona, the SURFRAD suite of instruments includes an MFRSR. A sky camera of the model TSI (Total Sky Imager) from Yankee Environmental Systems (YES) takes sky images at 1-minute time steps.

The two locations are middle-latitude, Northern Hemisphere sites. However, they hold some geographic and climatic differences that make pertinent the use of data from both sites in the current research. First, Girona is at low altitude and close to the sea, while Boulder is at high altitude and thousands of km away from the closest coast. Therefore, climate in Boulder is much more continental, in the sense that warmer summers and colder winters are likely; more important here is that the atmosphere above Boulder is in general drier and cleaner, so different cloudiness regimes and lower aerosol load are expected. Dominant aerosol types at the two sites are likely different too, with maritime aerosol and Saharan dust relatively usual at Girona, and continental dust and wildfire smoke more common at Boulder."

3. Methods

Raw measurements and observations from the above instruments need to be processed in order to obtain quantitative or qualitative information about the sky condition, clouds and/or aerosol. In all processing and algorithms used (and explained below) decisions must be taken to distinguish between clear sky (either clean or with a certain aerosol load) and clouds, or between clouds and aerosol. These decisions usually take the form of thresholds, which are somewhat subjectively selected after some tuning procedure. Sometimes, the human intervention is obvious, for example when deciding which sky images are considered as cloudless references. In the next paragraphs, we will explain the standard methods applied to raw data, and will describe the sensitivity analyses that we have performed on them to reach our goal.

Broadband solar radiation measurements at high temporal resolution (< 5 minutes) can be used to infer the sky conditions. In this regard, after some initial attempts (Calbó et al., 2001; Duchon and O'Malley, 1999) a Radiative Flux Analysis (RadFlux) technique was developed to provide quantitative sky cover characteristics (Long et al., 2006a; Long and Ackerman, 2000) and is currently quite broadly used. Updated versions of this methodology also make use of longwave irradiance measurements (Long and Turner, 2008) and of other meteorological variables; here we will focus, however, on the use of solar radiation measurements. In summary, the method comprises two steps. The first step (Long and Ackerman, 2000) consists in identifying clear (i.e., totally cloudless) instances within a time series of solar radiation data. Several conditions must be met: primarily global irradiance must be between certain limits, diffuse irradiance must be less than an imposed threshold, global irradiance must show low variability, and the ratio of diffuse to global solar irradiance must also have low variability. These conditions are applied to "normalized" values (i.e., the cosine and the longer path effects due to changing Sun's position are removed). On the basis of the identified clear sky periods within the time series, empirically adjusted clear-sky estimated values of global, direct, and diffuse irradiances are computed for the whole time series, regardless of sky condition. In the second step (Long et al., 2006a) the daylight fractional sky cover (*fsc*) is estimated based upon the “diffuse cloud effect,” i.e., the ratio of the difference between measured diffuse irradiance and the estimated clear-sky diffuse irradiance normalized by the estimated clear-sky global irradiance. It should be noted that other conditions are also applied to identify totally overcast and totally cloudless instances.

Although several empirically or subjectively given parameters are used within these algorithms, the most relevant one regarding the differentiation between thin clouds, aerosols, and a clean sky is the maximum diffuse irradiance that is admissible for clear skies. The diffuse irradiance is produced by scattering, thus this setting limits how much scattering is allowed for skies to be classified as “clear.” Indeed if the Max_Diff parameter is set to a very low value, such as that for Rayleigh (molecular) scattering in the atmosphere, it is likely that very few instances would be identified as clear. Similarly, when estimating cloud cover, cases with heavy aerosol loading that produces large amounts of diffuse irradiance will be considered as cloudy situations. If it is fixed to a too high value, cases with thin clouds may be considered clear. In the original paper, Long and Ackerman (2000) suggested a value around 120-150 W m^{-2}. Below we analyze the effect of changing this threshold on clear sky determination and fractional sky cover estimation.

As its name indicates, the MFRSR uses a rotating shadowband to consecutively shade and unshade the detector. In this way, direct (beam) radiation on the horizontal surface of the detector is estimated by subtracting the shaded diffuse measurement from the corresponding unshaded global measurement. These inferred beam measurements, if their value is greater than zero, are then processed for aerosol optical depth. As explained in many papers (Harrison and Michalsky, 1994; Michalsky et al., 2010; Sanchez-Romero et al., 2016), this process has several steps, including continuous Langley calibration of the spectral sensors, evaluation of total optical depth, subtraction of Rayleigh and ozone extinction, and –more importantly here– cloud screening. Thus, after the first three steps, an optical depth (OD, that might be due to water droplets or ice crystals, or aerosol particles, or both) for each wavelength but the longest (940 nm), which is affected by water vapor absorption, is computed. Using two of these values (OD at 500 and 870 nm) the Ångström exponent, that accounts for the wavelength variation of OD and varies inversely with the particle size, is also estimated. These values then must go through scrutiny to distinguish those that actually correspond to the effect of aerosols in the atmosphere from those which are affected by (necessarily) thin clouds. Obviously, a number of cases correspond to situations that cannot be clearly identified as either clouds or aerosol, but in general, the cloud screening procedures routinely implemented are conservative in the sense that they tend to guarantee that the filtered cases are free of “cloud contamination.”

There are in the literature several suggestions for cloud screening the OD data from MFRSR. The SURFRAD network applies the technique described in Augustine et al. (2008) that is a hybrid of the cloud screening methods of Michalsky et al. (2010) and Alexandrov et al. (2004). As in the case of identifying clear skies from solar radiation data, the variability of the measurement is the basis of all methods: the underlying assumption is that clouds make solar radiation (either broadband or spectral) more variable in time than aerosols. Here we will use the methodology as presented by Michalsky et al. (2010), which consists of two filters applied consecutively on a moving time window of a given width (10 minutes in the original paper). The first, coarser filter takes the difference between each adjacent measurement, and also calculates the maximum minus the minimum OD in the window. If all differences are less than a given threshold, and if the range of measured OD within the time window is less than another threshold, then the points pass the first filter. The second, more stringent filter scales the allowed variability according to the magnitude of the OD, which is estimated by applying a low-pass filter on the series. Thus, the absolute value of the largest difference between adjacent data must be less than a given fraction of the estimated OD at the midpoint of the sample window, and the range must be less than another fraction of the same estimate. The values of the four thresholds were 0.02 and 0.03 (absolute differences of OD at 550 nm) and 10 and 20% respectively in the original paper. In the present study, we will change these four values, and also the time window where differences and ranges are calculated, to assess their effect regarding “transition” cases. The final result of the MFRSR cloud screening is every sample tagged as “good” or “bad,” meaning that can be representative of aerosols or not. In the current paper, we will assume that samples labeled as “bad” correspond to the presence of some kind of clouds.

As mentioned above, images of the whole sky are becoming more ubiquitous both in atmospheric research and in solar energy management applications. Automatically captured sky images allow a continuous (many such cameras take images every minute or even more often) visible record of the sky. Images can then be visually scrutinized to identify clouds, aerosols, rain, and any other meteors. Usually, however, an automatic digital image analysis is set to obtain an estimation of the fractional sky cover and (sometimes) other sky or cloud characteristics. In the present research, one year of 1-minute sky images taken at Girona have been visually inspected and tagged according the presence of situations where the distinction between clouds and aerosols is unclear. In addition, one year of 1-minute images taken by the TSI at Table Mountain have undergone digital processing to account for the fractions of sky that is free of cloudiness, or covered by optically thin and thick clouds. The basis of the distinction is the ratio between the red and the blue intensities (R/B) in the RGB image: a clear (blue) pixel has a low value of R/B, while a cloud (white) pixel has a greater value. In this case, the process uses mainly two R/B thresholds referenced to the baseline clear-sky threshold set by the manufacturer to make these distinctions: one to distinguish between clear sky and thin cloud, a second one to separate between thin and thick clouds. As explained elsewhere (Long, 2010; Long et al., 2006b), a post-image-processing algorithm addresses issues in regions of particular difficulty (a circle around the Sun, the region close the horizon in the direction of the Sun), which occur due to forward scattering of visible light by aerosols and haze, and the intensity range limitations of the detectors of the cameras used to record the sky images. But in our analysis, we have focused mainly on the threshold that affects the distinction between clear sky (with more or less aerosol content) and thin clouds.

4. Results

4.1 Clear sky detection and cloud cover estimation from radiation flux analysis

RadFlux analysis results for Girona, 2014 are presented below. The analysis was applied twice, with values of Max_Diff equal to 100 and 200 W m^{-2}. We also checked the value of 300 W m^{-2}, but those results were nearly the same as those for the 200 W m^{-2} setting, indicating that when such high values of diffuse radiation are in principle set to correspond to clear sky, other tests for clear-sky detection filter out these cases anyway. It should be noted that even with the lower threshold, the diffuse irradiance allowed as "clear sky" is well above the Rayleigh limit, i.e., a certain amount of scattering particles larger than molecular is always allowed. A summary of results is presented in Table 1. There are almost 11,000 minutes identified as clear when the higher threshold is used but labeled as not clear when the lower threshold is applied. This means that almost 5% of the daylight hours (specifically, of the time when the Sun is more than 10° above the horizon, a condition for the RadFlux algorithm to identify clear skies), may be considered clear or not depending on where we set the maximum allowed diffuse limit. These situations often correspond to what can be generically called "haze," that is conditions that can hardly be classified as either cloud or dry aerosol. For Boulder, results are similar. More than 15,000 minutes (7.5%) are considered clear or not depending on the Max_Diff value (here the two tested values were 100 and 180 W m^{-2}).

The difference in mean *fsc* when data are processed with one or the other threshold is 0.023 (0.022) in Girona (Boulder). This difference might not seem very large, but, as we will show below, it is produced by larger differences for some particular conditions. Thus, differences between the mean *fsc* when one or the other clear sky reference is used (i.e. based on clear sky periods identified by using one or the other Max_Diff value) increase significantly when cloudless and overcast conditions are not considered. Indeed (see Table 1), for scattered to broken cloud conditions, the average difference is 0.044 (0.046), which is more than 10% of the average *fsc* of about 0.4 at both sites. Logically, since RadFlux uses the difference between measured and estimated clear-sky diffuse as the basis for *fsc* estimation, estimated *fsc* tends to be lower when Max_Diff is greater. In absolute value, differences tend to be greater for lower *fsc* (see Figure 1 corresponding to Girona data). Table 2 summarizes the number of records with significant differences in *fsc*. It is worth noting that for about 15,000 (17,000) minutes the difference is greater than 0.10. This means that in about 14% (17%) of non-cloudless and non-overcast cases, the average difference of *fsc* is a relatively high value of 0.16 (0.15).

We will next present the evolution of solar radiation and results of RadFlux (and also from MFRSR) for some particular days, as examples of the behavior of the algorithm with regard to the objectives of the present research. The mean values of *fsc* for these days when using the two Max_Diff values are shown in Fig. 1. Figure 2 presents in detail measurements and processed results for two days that, based on visual inspection of the images (see Figure 3) and the RadFlux with the greater threshold, are considered to be clear. March 6, 2014, is an example of a cloudless and very clean atmosphere day. Measured diffuse and direct (projected onto a horizontal surface) irradiances match almost exactly their clear sky estimates. It should be noted that for this day, no significant difference exists between the estimate of clear sky diffuse irradiance after using one or the other threshold of Max_Diff. As a consequence, for this day, the estimate of *fsc* is zero, whatever the threshold used. Consistently, the MFRSR cloud screening algorithm flagged almost all minutes as "good" (i.e., not contaminated by clouds), and the OD at 500 nm is less than 0.1 for the whole day, while the Ångström exponent (AE) evolves between 1 and 2, indicating relatively small particles. For June 21, 2014, both diffuse and direct irradiances follow a relatively smooth evolution that matches the clear sky estimates quite well. For diffuse, this is true if the clear sky estimate corresponds to the higher threshold. Therefore, if the higher Max_Diff is used, the RadFlux produces an almost cloudless day (*fsc* is very close to zero, with a daily average of 0.02). In contrast, when a Max_Diff = 100 W m^{-2} is used, not a single minute is considered clear, and the *fsc* is estimated to be between 0.2 and 0.4 (daily mean, 0.27). As mentioned above, however, there are no "visible" clouds in the sky, and in fact, the MFRSR cloud screening algorithm labels all records of this day as "good." Nevertheless, the AOD for this day is relatively high (0.15-0.30) and, more significantly, the AE is low (0.4-0.9) indicating, as suspected, larger (and/or hydrated) particles.

Two particular cases of days with variable cloudiness are presented in Figure 4: one presents almost exactly equal *fsc* estimations, while the other presents notable *fsc* differences between the two estimations. As can be seen in the corresponding sky images (Figure 5), the first day (April 24) shows middle and high clouds, and low aerosol load, which is confirmed by the MFRSR OD data: for the times that pass the cloud screening, OD is around 0.15 and AE is around 1.5. But the second day (June 23) has low level clouds in a more "whitish" sky, which results from a greater OD (0.25) and lower AE (< 1).

4.2 MFRSR estimations of OD and AE, and cloud screening

Figure 6 shows the behavior of the Ångström exponent versus the optical depth at 500 nm, for all instantaneous measurements that are processed by the MFRSR algorithm, that is for all instances when there is some direct irradiance and the solar zenith angle is less than 80°. These are measurements from Girona for the year 2014. The whole unscreened dataset of measurements are represented by black circles. It should be noted that plotted is the optical depth of whatever is in the atmosphere (other than well-mixed gases and ozone) as we don't know, in principle, if this optical depth is due to dry particles, water droplets or ice crystals. There are many points with negative values of AE, which must be the result of the uncertainties of the method to estimate AE. As shown by Sanchez-Romero et al. (2016), the uncertainty attached to AE computation is of the order of 0.5 for OD values of about 0.1, and greater for lower OD values. Therefore, when the true value of AE should be close to 0, the random error associated with this uncertainty may result in negative values. A deeper analysis of the effect of OD measurement errors on the computation of AE that explains how negative AE values may be obtained, was developed by Wagner and Silva (2008). Their results discourage the computation of AE when OD is less than 0.15, given the typical uncertainties of the current instrumentation. That same study shows that the error in the AE estimation may be skewed depending on the relative errors of each of the monochromatic ODs used.

The data points highlighted in red in Fig. 6 are all those that have passed the cloud screening filter (i.e., labeled as “good”). Initially (Fig. 6a) we used the same time window and threshold values for cloud screening as suggested in Michalsky et al. (2010). Subsequently, we changed these values as summarized in Table 3. Changing the time window means that the filter would take into consideration the variability of the computed OD over a shorter or a longer period. Changing the other thresholds would mean that the filter accepts aerosol conditions that show more or less variability. With the default cloud screening, 42% of points are considered representative of atmospheric aerosol. Most of these points have OD < 0.5 and AE between 0 and 2. The sensitivity analysis showed that shortening the time window has an important effect of allowing more points to be considered aerosol. In contrast, lowering the thresholds corresponding to relative values of differences and range substantially reduces the number of points that pass the filter. We combined a shorter time window and higher values of the thresholds to apply a “relaxed” cloud screening or conversely a longer time window and lower thresholds to produce a more “strict” filter. When the former is applied, almost 58% of points are considered aerosol (Fig. 5b), but when the latter is used, less than 19% of the points pass the filter (Fig. 5c). With very few exceptions, all points with OD > 1.0 and most points with negative AE (and OD > 0.1) do not pass the cloud screening even with the relaxed filter.

The numbers in Table 3 allow an estimation of the frequency of transition cases between cloud and “pure” aerosol. We start with about 420,000 instantaneous measurements for Girona performed by the MFRSR with solar zenith angle less than 80° (it should be noted that this number is a combination of 1-min measurements during 9 months plus 15-sec measurements during 3 months). From these, about 212,000 (50.5%) are not processed by the MFRSR, due to the presence of clouds thick enough to occult the Sun and to preclude obtaining valid optical depth results. From the rest of the samples (208,000) about 88,000 additional points must be considered clouds, as even the most relaxed cloud screening labels them as “bad.” Therefore, in about 70% of instances, there are clouds (either optically thick or thin) in front of the Sun. This “cloud occurrence” might be eventually an estimation of the mean cloudiness, but it should be noted that only clouds that are in front of the Sun from the perspective of the MFRSR are considered by the cloud screening algorithm, so it is not a hemispheric view of the sky. In other words, whereas the clear sky identification from the RadFlux refers to the whole hemispheric sky view, the cloud screening for the MFRSR refers only to the direct sun, not the whole sky. From the rest of the samples, we can almost assure (according to the result of applying the “strict” cloud screening) that about 39,000 data points correspond to clear sky (in the direction of the Sun beam) affected by a certain amount of aerosols. This means that about 81,000 measurements (19% of the initial number) are affected by particles in the atmosphere that are problematic in being classified as aerosol or as cloud, at least based on the cloud screening applied which is built upon the assumption that clouds induce higher variability than aerosols in the measured irradiances.

The discussion above concerns results from Girona. When the same analysis is applied to measurements from Boulder, the numbers obviously change, but not the main result of a large percentage of cases in the transition zone. We started with 610,000 instantaneous measurements (note that 20-sec resolution was used in Boulder for the whole year) from which about 158,000 (25%) were not processed by the MFRSR, due to thick clouds occulting the Sun. Then we applied the three cloud screenings (default, relaxed, strict) to the rest of the samples (452,000, see Table 3). About 242,000 additional points were labeled as "bad" (i.e. clouds) by the relaxed cloud screening, so in a total of 66% of instances there are clouds before the Sun (note the important difference between the number of thick and thin clouds as compared with Girona). From the remaining data, about 37,000 data points correspond to a cloudless sky affected by aerosols. This means that about 173,000 measurements (28% of the initial total) correspond to the kind of particle suspension that represents the transition region between aerosols and clouds, at least regarding the observations by the MFRSR, which are mostly affected by what is present in the direction of the Sun.

Again for Girona and for the four days analyzed in Figs. 2 and 4, Figure 7 presents the periods that passed the MFRSR cloud screening (i.e., the calculated OD is considered to be due to aerosols) for the three different settings (default, strict, relaxed). The first two days are considered cloudless by the default screening (and obviously, by the relaxed one), and also mostly cloudless by the strict screening. Somewhat surprisingly, a period of the first day (10:00-11:30 approximately) is filtered out by the strict screening, owing to a relatively high variability of the signal despite that sky images and the RadFlux analysis indicate that this is a totally cloud free, clean day. Conversely, the second day raises some doubts about what it is in the air according to images and RadFlux, but is considered almost totally cloudless even by the strict MFRSR screening.

With all this in mind, we find that the variability of the optical depth (which is intended to reflect the variability in the atmosphere, although we cannot rule out some contribution from the instrument's noise when the signal is very low) is not sufficient to discriminate between cloud and aerosol. The optical depth itself and its wavelength dependence (AE) do not help very much in this distinction (despite that Kassianov et al. 2013 suggested a method that worked well for their Arctic site). Figure 8 shows the histograms of the populations of points screened out as clouds (this is for Girona, so 88,000 points), points that passed the strict filter so they are considered aerosol (39,000), and points that belong to the transitional zone (81,000), as a function of OD and AE. It is obvious that the filter does a good job as the dominant OD and AE values for clouds and aerosols respectively are quite different among them (despite some data with large AE is labeled as cloud, and other minor inconsistencies are found as well). But it is also apparent that the third group of points presents values of OD and AE that cover a very broad range. Even if we assume that all points with OD < 0.032 or AE > 1.6 must be considered aerosols, and all points with OD > 0.32 or AE < 0.15 must be considered clouds (these values derived from the percentiles 1 and 99 of the distributions of cloud and aerosol points), there are still about 58,900 points within the range of OD [0.032-0.32] and AE [0.15 – 1.6] for which their corresponding variability is not either high enough to be considered clouds nor low enough to be considered aerosols without some doubts. This number represents 14% of the initial measurements and 28% of the instances processed by the MFRSR. The corresponding relative values for Boulder data are 10.7% and 14.5%. It should be noted that the previous thresholds for OD and AE, based upon the statistical distributions of our data, must not be taken for general application to all atmospheric situations. For example, Antón et al. (2012) found a very large OD (0.8-1.5) and very low AE (0.1-0.25) under a strong Saharan dust event.

4.3 Images from sky cameras

For Girona, there are about 200,000 total sky images corresponding to 341 days during the year 2014. The most significant gap in the series of sky images corresponds to the first fourteen days of the year (there are also some missing days in April and June). Since visually inspecting each and every one of these images is unfeasible, we built a movie for each day by displaying all images successively. Watching these movies is much more practical, and allows identifying the most important features in the images. Once some particularly interesting days or periods within a day were selected, the individual images were visually inspected in more detail. Some examples of these images have already been used to discuss previous results (see Fig. 3 and Fig. 5). Overall, there is a high percentage of days when we have detected some period (that may last less than one hour or may last the whole daylight time) of challenging distinction between clouds and aerosols (40% of days). Indeed, most of the other days (those without doubtful periods) correspond to mostly overcast days, or, exceptionally, to unusually clear days. Regarding the challenging periods, there are a few different situations. First are relatively clean and apparently cloudless skies where a kind of a thin "veil" can be seen in the images, without an analyst being able to subjectively discern whether it is made up of dry aerosols or extremely thin clouds (either low or high). Second are hazy or foggy skies with corresponding difficulties in affirming what kind of suspension is causing the haziness. Third are skies with scattered or broken clouds (typically, cumulus) that have poorly defined boundaries or are continuously forming and vanishing, which makes it difficult to decide whether a portion of the sky is cloudless or not.

We have been able to perform a more quantitative analysis on TSI images from the Boulder site. In 2014, there are 217 days with images every 1 minute, which translates to 145,000 images being processed. The missing periods correspond to most of January, April, and July, with some additional missing days randomly distributed across the other months. Main reasons for missing images are a malfunctioning camera or rotating mirror, but sometimes the outages are due to inclement weather. The original processing of the images produced an average cloud fraction of 0.62 of which 0.13 is considered thin cloud (again, in average for all images). These numbers are the result of using the SURFRAD operator settings in the TSI image processing for the Table Mountain site, i.e. a nominal R/B threshold between clear sky and thin clouds of 0.30 and an effective threshold between thin and thick clouds of 0.57. To test the sensitivity of the cloud fraction results to the first threshold, we first lowered it to 0.20, and then raised it to 0.40. This produced, respectively, an increase in average *fsc* to 0.68, and a decrease to 0.57, mainly due to the change of the amount of thin clouds (since we kept the thin to thick cloud threshold the same). It should be noted that the range of total cloud fraction from TSI estimates (0.57-0.68) is relatively close to the estimate from the Rad_Flux (0.54-0.56) and to the cloud occurrence found by the MFRSR (0.66), with the difference likely mostly related to the circumsolar and near horizon issues described in Long

(2010) and Long et al. (2006b), besides different field of view (for MFRSR) and slightly different periods (due to missing data or images).

More important than these aggregate numbers is to look at the particular cases with large (or small) cloud fraction changes when the threshold is changed. In this sense, Table 4 shows the differences in thin cloud fraction between the original processing and new processing using two modified thresholds. For the case of the reduced threshold, the thin cloud fraction estimate in almost 80% of images increases by less than 0.10. This of course includes those images that presented a very high cloud fraction (overcast, or almost overcast), but there are also a large number of images for which the change is very small independently of their cloudiness. This illustrates the robustness of the digital image processing of TSI images, i.e., it shows that even if the "correct" threshold is unknown, the cloud fraction estimate is, in general, quite consistent. Figure 9a presents an example of these cases: a totally cloudless image, which is considered as such even by the lower threshold used. Similarly, Fig. 9b shows a broken cloud sky, where again changing the threshold does not affect the result as the clouds have very well defined limits and the sky is very clean (blue). On the other extreme, more than 20% of images exhibit a change in the estimate of the thin cloud fraction greater than 0.10 with the changing thresholds. It should be noted that this increase is not always reflected in an equivalent increase of the total cloud fraction, since the sophisticated algorithm that sets the particular thresholds that are used in each region of each image may result in slight changes of the opaque cloud fraction too. Fig. 9c shows a sample of an image where the change in the threshold produces a large change in the thin cloud fraction, because a large part of that image is made up of what seems very thin clouds. In the example of Fig. 9d, the large differences seem to be related to a relatively high atmospheric aerosol load.

For the case of the increased threshold, the thin cloud fraction estimate in a little more than 80% of images decreases by less than 0.10 (Table 4). This includes a) some situations of cloudless skies, b) situations with scattered to broken cloudiness but with a low amount of thin clouds (in these two cases, the increase of the threshold of course makes it impossible to get lower cloud fractions), and c) situations of overcast skies with thick clouds, that present much higher values of the red to blue ratio (or that are set as cloudy because of very low light intensity, i.e., very thick clouds). Again, this result confirms that the method is quite robust, and also that almost 20% of time a change in the threshold produces a change in the thin cloud fraction of more than 0.1. In Figures 9a-f the result of the cloud identification with the higher threshold is also displayed, and we can see the moderate effect on cases of Fig. 9c and 9d, corresponding to clouds (or aerosols) with not well defined limits and that are mainly visible when they are in front of the Sun due to their forward scattering characteristics. The greatest effect of changing the threshold is found in situations such as those presented in Fig. 9e and 9f, where the hazy atmosphere (involving cumulus clouds formation) is too problematic to be classified as "clear" or "cloudy" with thin or even opaque clouds by the method applied to TSI raw images. It should be noted that in the cases where the effect of changing the threshold is small (Fig. 9a and 9b), the optical depth as measured by the MFRSR was also very low (around 0.02), while for the rest of cases (Fig. 9c-f) the optical depth (in the nearest periods when is available) is always greater than 0.1 and in fact, close to

0.2, which is the value that Dupont et al. (2008) found as the limit related to the more common differentiation between cloud and not cloud.

5. Discussion, summary and conclusion

We have presented observations from three ground based, passive systems, that are intended to detect clouds and aerosols in the atmosphere. Indeed the three systems share one characteristic, which is that they are sensitive to the solar radiation flux once it has been modified (affected) by the presence of suspended particles in the air (of course, solar radiation flux is also affected by atmospheric gases). Thus, sky cameras “map” radiation coming from the whole sky dome and record this radiation in three color channels (red, green, blue). The presence in the intervening atmosphere of particles (whether in the form of clouds or aerosol) modifies the aspect of the sky, that is the partitioning of light corresponding to each color. Broadband radiometers perceive the effect of clouds and aerosols as these modify the total amount of solar radiation reaching the ground, and/or the partitioning of radiation between the direct and diffuse components. Finally, the MFRSR determines the effect on the direct solar beam so it can estimate the optical depth resulting from the absorption and scattering (i.e. attenuation) phenomena associated with the suspended particles. Since the latter is a spectral instrument, it can be used to evaluate optical depths for several wavelengths and therefore, the variation of the optical depth with wavelength, which is related with the size and characteristics of the particles.

The general conclusion of the analyses performed here is that the number of challenging cases where distinction between aerosol and cloud is nebulous (in fact, only subjectively resolved) is not negligible, for at least the two mid-latitude sites analyzed and for the instruments used. A very rough estimate of the frequency of instances when the mentioned cloud-aerosol distinction is challenging is a figure not less than 10%. This number includes those cases that are cloudless in principle, but with a very thin veil in the sky that is hardly visible but affects the partitioning of the solar radiation in the diffuse and direct components (5 and 7.5% of time according to RadFlux in Girona and Boulder respectively, Section 4.1). This gross estimate also includes cases with scattered and broken clouds, when the cloud limits are not very definite, or when there is a suspension that somewhat attenuates the direct beam in the “clear” patches between clouds. According with the MFRSR datasets and applied analyses, the lowest estimates of these situations at Boulder and Girona respectively are 10.7 and 14% (Section 4.2). In all these cases the spectral signature of solar radiation is also affected, which is reflected in the computation of the Ångström exponent. These numbers are also in agreement with what we find from the sky images. The sensitivity analysis performed showed that changing the threshold that distinguishes clear sky and thin cloud, which is essentially how “whitish” the cloud-free sky (includes cases with relatively high aerosol) is allowed to be, produces large differences (in the “thin” cloud fraction) a significant amount of time. Specifically, we find a change in the thin cloud fraction of more than 0.1 in about 20% of images (Section 4.3). This latter result is for Boulder, but for Girona, a visual inspection of images suggests similar results.

These values are quite in agreement with the few previous numbers given in the literature, although they are not directly comparable. Indeed, Koren et al. (2007) estimated that between 30 and 60% of the part of the globe at any given time considered to be free of clouds could correspond to the challenging characteristics transitioning between clouds and aerosols (which they called "twilight zone"). Similarly, for a particular area of the Atlantic Ocean, Bar-Or et al. (2010) found a value of about 35-45%. In these latter studies, a spatial approach was considered, i.e., they accounted for the extension of this zone in a snapshot of the sky. Our study, however, combines this approach (for sky camera images and partially for broadband hemispheric solar radiation measurements) with a temporal approach, that is accounting how often the atmosphere presents a state that cannot be distinctly categorized as cloud or as aerosol (for broadband hemispheric radiation measurements and also for MFRSR, Sun pointing, measurements). Therefore, our numbers correspond mainly to temporal frequencies, are limited to two particular sites, and are quite conservative, but if we discard the overcast conditions, the relative frequency of the transition cases increases to more than 15% of the remaining cases (this number is estimated by dividing the above overall value of 10% by the frequency of non-overcast cases, which is about 70% at the two involved sites).

Our results support the argument that clouds and aerosol are two extreme manifestations of the same physical phenomenon, which is a suspension of particles in the atmosphere. This reasoning was already suggested by other authors (e.g., Charlson et al. 2007). This of course could be questioned, as the origin and the many processes involved differ quite a lot. On the one hand, processes involved in producing different types of aerosols such as sea salt spray, secondary pollutant particles, forest fire smoke, and desert dust, may be quite different. Also different are processes leading to the formation of different types of clouds: for example maritime thin stratus, cumulonimbus, or high ice clouds. Therefore, we can conclude that a suspension of particles in the air may have many different origins, compositions, properties, etc., but, despite their differences of origin and composition, their radiative effect as seen from the ground does not easily distinguish the type of suspension. In particular, at times we cannot classify the suspension in either of the two most usual cases: clouds (relatively large condensed water particles) and aerosols (relatively small dry particles). Difficulties in separating these cases may result from the fact that the instruments have a hemispheric view of the sky (pyranometers, cameras) which may integrate radiation fluxes (radiances) that, separately, could be distinctly affected by clouds or aerosols. Or even in the case of directional measurements (such as the MFRSR measurements), the solar beam attenuation that is obtained is the result of the light crossing through different layers of the atmosphere which may contain a cloud at some height and suspended aerosols at other heights.

Many cases may correspond to a situation where the particles in the suspension show characteristics (size and composition) that are somewhere in between what is typically considered cloud and aerosol. In these situations, it might not make sense trying to classify the suspension as a cloud or aerosol. Rather, it might be more convenient to treat the phenomena as a continuum, of which the extremes would be the entities corresponding to the usual definitions of cloud and aerosol, but with a non-negligible number of intermediate conditions (Charlson et al., 2007). The two most common situations with the characteristics in the “middle” of the continuum are those with clear skies with a thin veil showing some sort of structure, and those with partly cloudy skies with poorly defined cloud boundaries (Koren et al., 2008, 2009).

Although other active cloud observation instruments (such as ceilometers, radars, microwave radiometers) do provide more detailed information on cloud structure and particles forming the clouds, they in fact also support the case of a continuum of properties, and of the difficulty in setting precise limits on what must be labeled as a cloud (Boers et al., 2010). Similarly, the use of radiance measurements in several directions of the sky dome, as for example those performed by CE-318 sunphotometers (CIMEL Electronique, France), can map the presence of clouds in selected planes so helping in the detection of clouds and the distinction from pure aerosol. The quantification of the transition situations as seen from these other instruments could be a matter of future research.

As for the consequences of the above conclusions and suggestions, we think that considering the intermediate situations between cloud and aerosol may have a significant impact in energy balance studies, either local or global, and must be taken into account when parameterizing radiation transfer within weather and climate models. The point here is that cloud-screening algorithms for aerosol products and cloud detection algorithms for cloud products both tend to be conservative, which bias both sets of products in a way that the transition area is maximally omitted from products. For example, when considering scattered cloud conditions, assuming that there are, or are not, condensed particles in the patches between clouds will produce different downward and upward radiation fluxes (both in the solar and in the thermal infrared bands), that would be different also from what is actually observed by radiometers on the ground. The properties of the suspended particles that are around or between the clouds are also relevant where radiation transfer is concerned (Schmidt et al., 2009). High spatial resolution observations of cloud boundaries, such as in Schwartz et al. (2017) where cloud structure is examined on scales 3 to 5 orders of magnitude finer than satellite products, or high temporal sampling of radiation spectra at cloud boundaries by using array spectrometers (González et al., 2017), open new paths for examination the cloud-aerosol conundrum. Even if a homogeneous stratified atmosphere is assumed in a given region, considering that there is a layer of a very thin cloud or a layer of aerosol particles having differentiated radiative properties may also result in different estimates of the radiation fluxes. If possible, it would be more realistic and accurate to treat the phenomenon as a continuum in the radiative transfer calculations. Despite the existence of several studies that already address some of these concerns (Charlson et al. 2007; Koren et al. 2008, 2009; Hirsch et al. 2012, 2014; Yang et al. 2016), all these subjects must be the object of further research.

Acknowledgements

This research is developed within the framework of the project NUBESOL (CGL2014-55976-R) which is funded by the Spanish Ministry of Economy and Competitiveness. The work was mostly carried out while the first author was enjoying a research stay at NOAA-ESRL-GMD, which was partly funded by the Spanish Ministry of Education, Culture and

Sports, through grant PRX16/00161. Many people from the Global Radiation Group at NOAA-ESRL GMD assisted in this research by providing data, software, and in particular, expertise and educated insight.

References

Albrecht, B.A., 1989. Aerosols, cloud microphysics, and fractional cloudiness. Science (80-.). 245, 1227–1230. doi:10.1126/science.245.4923.1227

Alexandrov, M.D., Marshak, A., Cairns, B., Lacis, A.A., Carlson, B.E., 2004. Automated cloud screening algorithm for MFRSR data. Geophys. Res. Lett. 31, 1–5. doi:10.1029/2003GL019105

Antón, M., Valenzuela, A., Cazorla, A., Gil, J.E., Fernández-Gálvez, J., Lyamani, H., Foyo-Moreno, I., Olmo, F.J., Alados-Arboledas, L., 2012. Global and diffuse shortwave irradiance during a strong desert dust episode at Granada (Spain). Atmos. Res. 118, 232–239. doi:10.1016/j.atmosres.2012.07.007

Augustine, J.A., DeLuisi, J.J., Long, C.N., 2000. SURFRAD—A National Surface Radiation Budget Network for Atmospheric Research. Bull. Am. Meteorol. Soc. 81, 2341–2357. doi:10.1175/1520-0477(2000)081<2341:SANSRB>2.3.CO;2

Augustine, J.A., Hodges, G.B., Cornwall, C.R., Michalsky, J.J., Medina, C.I., 2005. An Update on SURFRAD—The GCOS Surface Radiation Budget Network for the Continental United States. J. Atmos. Ocean. Technol. 22, 1460–1472. doi:10.1175/JTECH1806.1

Augustine, J.A., Hodges, G.B., Dutton, E.G., Michalsky, J.J., Cornwall, C.R., 2008. An aerosol optical depth climatology for NOAA's national surface radiation budget network (SURFRAD). J. Geophys. Res. Atmos. 113, 1–13. doi:10.1029/2007JD009504

Bar-Or, R.Z., Koren, I., Altaratz, O., 2010. Estimating cloud field coverage using morphological analysis. Environ. Res. Lett. 5, 14022. doi:10.1088/1748-9326/5/1/014022

Boers, R., De Haij, M.J., Wauben, W.M.F., Baltink, H.K., Van Ulft, L.H., Savenije, M., Long, C.N., 2010. Optimized fractional cloudiness determination from five ground-based remote sensing techniques. J. Geophys. Res. Atmos. 115, 1–16. doi:10.1029/2010JD014661

Calbó, J., González, J.-A., Sanchez-Lorenzo, A., 2016. Building global and diffuse solar radiation series and assessing decadal trends in Girona (NE Iberian Peninsula). Theor. Appl. Climatol. doi:10.1007/s00704-016-1829-3

Calbó, J., González, J.A., Pagès, D., 2001. A method for sky-condition classification from ground-based solar radiation measurements. J. Appl. Meteorol. 40, 2193–2199.

Calbó, J., Sabburg, J., 2008. Feature Extraction from Whole-Sky Ground-Based Images for Cloud-Type Recognition. J. Atmos. Ocean. Technol. 25, 3–14. doi:10.1175/2007JTECHA959.1

Cazorla, A., Olmo, F.J., Alados-Arboledas, L., 2008. Using a Sky Imager for aerosol characterization. Atmos. Environ. 42, 2739–2745. doi:10.1016/j.atmosenv.2007.06.016

Charlson, R.J., Ackerman, A.S., Bender, F.A.M., Anderson, T.L., Liu, Z., 2007. On the climate forcing consequences of the albedo continuum between cloudy and clear air. Tellus, Ser. B Chem. Phys. Meteorol. 59, 715–727. doi:10.1111/j.1600-0889.2007.00297.x

Chiu, C., Marshak, A., Knyazikhin, Y., Pilewskie, P., Wiscombe, W.J., 2009. Physical interpretation of the spectral radiative signature in the transition zone between cloud-free and cloudy regions. Atmos. Chem. Phys. 9, 1419–1430. doi:10.5194/acpd-8-17549-2008

Chiu, J.C., Marshak, a., Knyazikhin, Y., Wiscombe, W.J., 2010. Spectrally-invariant behavior of zenith radiance around cloud edges simulated by radiative transfer. Atmos. Chem. Phys. 10, 11295–11303. doi:10.5194/acp-10-11295-2010

Duchon, C.E., O’Malley, M.S., 1999. Estimating Cloud Type from Pyranometer Observations. J. Appl. Meteorol. 38, 132–141. doi:10.1175/1520-0450(1999)038<0132:ECTFPO>2.0.CO;2

Dupont, J.-C., Haeffelin, M., Long, C.N., 2008. Evaluation of cloudless-sky periods detected by shortwave and longwave algorithms using lidar measurements. Geophys. Res. Lett. 35, L10815. doi:10.1029/2008GL033658

Eck, T.F., Holben, B.N., Reid, J.S., Arola, A., Ferrare, R.A., Hostetler, C.A., Crumeyrolle, S.N., Berkoff, T.A., Welton, E.J., Lolli, S., Lyapustin, A., Wang, Y., Schafer, J.S., Giles, D.M., Anderson, B.E., Thornhill, K.L., Minnis, P., Pickering, K.E., Loughner, C.P., Smirnov, A., Sinyuk, A., 2014. Observations of rapid aerosol optical depth enhancements in the vicinity of polluted cumulus clouds. Atmos. Chem. Phys. 14, 11633–11656. doi:10.5194/acp-14-11633-2014

González, J.-A., Calbó, J., Sanchez-Romero, A., 2017. Measuring fast optical depth variations in cloud edges with a CCD-array spectrometer, in: AIP Conference Proceedings. American Institute of Physics, p. 4. doi:10.1063/1.4975534

Harrison, L., Michalsky, J., 1994. Objective algorithms for the retrieval of optical depths from ground-based measurements. Appl. Opt. 33, 5126–32. doi:10.1364/AO.33.005126

Harrison, L., Michalsky, J., Berndt, J., 1994. Automated multifilter rotating shadow-band radiometer: an instrument for optical depth and radiation measurements. Appl. Opt. 33, 5118. doi:10.1364/AO.33.005118

Heinle, A., Macke, A., Srivastav, A., 2010. Automatic cloud classification of whole sky images. Atmos. Meas. Tech. 3, 557–5667. doi:10.5194/amt-3-557-2010

Heintzenberg, J., 2012. The aerosol-cloud-climate conundrum. Int. J. Glob. Warm. 4, 219–241.

Hirsch, E., Agassi, E., Koren, I., 2012. Determination of optical and microphysical properties of thin warm clouds using ground based hyper-spectral analysis. Atmos. Meas. Tech. 5, 851–871. doi:10.5194/amt-5-851-2012

Hirsch, E., Koren, I., Levin, Z., Altaratz, O., Agassi, E., 2014. On transition-zone water clouds. Atmos. Chem. Phys. 14, 9001–9012. doi:10.5194/acp-14-9001-2014

Jeong, M.J., Li, Z., 2010. Separating real and apparent effects of cloud, humidity, and dynamics on aerosol optical thickness near cloud edges. J. Geophys. Res. Atmos. 115, 1–15. doi:10.1029/2009JD013547

Kassianov, E., Flynn, C., Koontz, A., Sivaraman, C., Barnard, J., 2013. Failure and redemption of multifilter rotating shadowband radiometer (MFRSR)/normal incidence multifilter radiometer (NIMFR) cloud screening: Contrasting algorithm performance at atmospheric radiation measurement (ARM) NSA and SGP sites. Atmosphere (Basel). 4, 299–314. doi:10.3390/atmos4030299

Kassianov, E., Ovchinnikov, M., Berg, L.K., McFarlane, S.A., Flynn, C., Ferrare, R., Hostetler, C., Alexandrov, M., 2010. Retrieval of aerosol optical depth in vicinity of broken clouds from reflectance ratios: Case study. Atmos. Meas. Tech. 3, 1333–1349. doi:10.5194/amt-3-1333-2010

Kazantzidis, A., Tzoumanikas, P., Bais, A.F., Fotopoulos, S., Economou, G., 2012. Cloud detection and classification with the use of whole-sky ground-based images. Atmos. Res. 113, 80–88. doi:10.1016/j.atmosres.2012.05.005

Koren, I., Feingold, G., Jiang, H., Altaratz, O., 2009. Aerosol effects on the inter-cloud region of a small cumulus cloud field. Geophys. Res. Lett. 36, L14805. doi:10.1029/2009GL037424

Koren, I., Oreopoulos, L., Feingold, G., Remer, L. a., Altaratz, O., 2008. How small is a small cloud? Atmos. Chem. Phys. Discuss. 8, 6379–6407. doi:10.5194/acpd-8-6379-2008

Koren, I., Remer, L. a., Kaufman, Y.J., Rudich, Y., Martins, J.V., 2007. On the twilight zone between clouds and aerosols. Geophys. Res. Lett. 34, 1–5. doi:10.1029/2007GL029253

Li, Q., Lu, W., Yang, J., 2011. A Hybrid Thresholding Algorithm for Cloud Detection on Ground-Based Color Images. J. Atmos. Ocean. Technol. 28, 1286–1296. doi:10.1175/JTECH-D-11-00009.1

Long, C.N., 2010. Correcting for Circumsolar and Near-Horizon Errors in Sky Cover Retrievals from Sky Images. Open Athmospheric Sci. J. 4, 45–52.

Long, C.N., Ackerman, T.P., 2000. Identification of clear skies from broadband pyranometer measurements and calculation of downwelling shortwave cloud effects. J. Geophys. Res. 105, 15609. doi:10.1029/2000JD900077

Long, C.N., Ackerman, T.P., Gaustad, K.L., Cole, J.N.S., 2006a. Estimation of fractional sky cover from broadband shortwave radiometer measurements. J. Geophys. Res. 111, D11204. doi:10.1029/2005JD006475

Long, C.N., Sabburg, J.M., Calbó, J., Pagès, D., 2006b. Retrieving Cloud Characteristics from Ground-Based Daytime Color All-Sky Images. J. Atmos. Ocean. Technol. 23, 633–652. doi:10.1175/JTECH1875.1

Long, C.N., Turner, D.D., 2008. A method for continuous estimation of clear-sky downwelling longwave radiative flux developed using ARM surface measurements. J. Geophys. Res. Atmos. 113, 1–16. doi:10.1029/2008JD009936

Marshak, A., Wen, G., Coakley Jr., J.A., Remer, L.A., Loeb, N.G., Cahalan, R.F., 2008. A simple model for the cloud adjacency effect and the apparent bluing of aerosols near clouds. J. Geophys. Res. 113, D14S17. doi:10.1029/2007JD009196

Marshak, A.L., knyazikhin, Y., Chiu, J.C., Wiscombe, W.J., 2009. Spectral invariant behavior of zenith radiance around cloud edges observed by ARM SWS. Geophys. Res. Lett. 36, 16802. doi:10.1029/2009GL039366

Michalsky, J., Denn, F., Flynn, C., Hodges, G., Kiedron, P., Koontz, A., Schlemmer, J., Schwartz, S.E., 2010. Climatology of aerosol optical depth in north-central Oklahoma: 1992–2008. J. Geophys. Res. 115, D07203. doi:10.1029/2009JD012197

Rosenfeld, D., Andreae, M.O., Asmi, A., Chin, M., de Leeuw, G., Donovan, D.P., Kahn, R., Kinne, S., Kivekäs, N., Kulmala, M., Lau, W., Schmidt, K.S., Suni, T., Wagner, T., Wild, M., Quaas, J., 2014. Global observations of aerosol-cloud-precipitation-climate interactions. Rev. Geophys. 52, 750–808. doi:10.1002/2013RG000441

Saito, M., Iwabuchi, H., 2016. Cloud Discrimination from Sky Images Using a Clear-Sky Index. J. Atmos. Ocean. Technol. 33, 1583–1595. doi:10.1175/JTECH-D-15-0204.1

Sanchez-Lorenzo, A., Calbó, J., Brunetti, M., Deser, C., 2009. Dimming/brightening over the Iberian Peninsula: Trends in sunshine duration and cloud cover and their relations with atmospheric circulation. J. Geophys. Res. 114, D00D09. doi:10.1029/2008JD011394

Sanchez-Romero, A., González, J.A., Calbó, J., Sanchez-Lorenzo, A., Michalsky, J., 2016. Aerosol optical depth in a western Mediterranean site: An assessment of different methods. Atmos. Res. 174–175, 70–84. doi:10.1016/j.atmosres.2016.02.002

Sanchez-Romero, A., Sanchez-Lorenzo, A., Calbó, J., González, J.A., Azorin-Molina, C., 2014. The signal of aerosol-induced changes in sunshine duration records: A review of the evidence. J. Geophys. Res. Atmos. 119, 4657–4673. doi:10.1002/2013JD021393

Schmidt, K.S., Feingold, G., Pilewskie, P., Jiang, H., Coddington, O., 2009. Irradiance in polluted cumulus fields : Measured and modeled cloud-aerosol effects. Geophys. Res. Lett. 36, L07804. doi:10.1029/2008GL036848

Schwartz, S.E., Huang, D., Vladutescu, D.V., 2017. High-resolution photography of clouds from the surface: Retrieval of optical depth of thin clouds down to centimeter scales. J. Geophys. Res. Atmos. 2898–2928. doi:10.1002/2016JD025384

Seinfeld, J.H., Bretherton, C., Carslaw, K.S., Coe, H., DeMott, P.J., Dunlea, E.J., Feingold, G., Ghan, S., Guenther, A.B., Kahn, R., Kraucunas, I., Kreidenweis, S.M., Molina, M.J., Nenes, A., Penner, J.E., Prather, K.A., Ramanathan, V., Ramaswamy, V., Rasch, P.J., Ravishankara, A.R., Rosenfeld, D., Stephens, G., Wood, R., 2016. Improving our fundamental understanding of the role of aerosol−cloud interactions in the climate system. Proc. Natl. Acad. Sci. 113. doi:10.1073/pnas.1514043113

Tapakis, R., Charalambides, A.G., 2013. Equipment and methodologies for cloud detection and classification: A review. Sol. Energy 95, 392–430. doi:10.1016/j.solener.2012.11.015

Ten Hoeve, J.E., Augustine, J.A., 2016. Aerosol effects on cloud cover as evidenced by ground-based and space-based observations at five rural sites in the United States. Geophys. Res. Lett. 43, 793–801. doi:10.1002/2015GL066873

Twomey, S., 1974. Pollution and the planetary albedo. Atmos. Environ. 8, 1251–1256. doi:10.1016/0004-6981(74)90004-3

Várnai, T., Marshak, A., 2012. Analysis of co-located MODIS and CALIPSO observations near clouds. Atmos. Meas. Tech. 5, 389–396. doi:10.5194/amt-5-389-2012

Várnai, T., Marshak, A., 2011. Global CALIPSO observations of aerosol changes near clouds. IEEE Geosci. Remote Sens. Lett. 8, 19–23. doi:10.1109/LGRS.2010.2049982

Várnai, T., Marshak, A., 2009. MODIS observations of enhanced clear sky reflectance near clouds. Geophys. Res. Lett. 36, L06807. doi:10.1029/2008GL037089

Wagner, F., Silva, A.M., 2008. Some considerations about Angstrom exponent distributions. Atmos. Chem. Phys. 8, 481–489. doi:10.5194/acp-8-481-2008

Wen, G., Marshak, A., Cahalan, R.F., 2008. Importance of molecular Rayleigh scattering in the enhancement of clear sky reflectance in the vicinity of boundary layer cumulus clouds. J. Geophys. Res. 113, 1–10. doi:10.1029/2008JD010592

Wu, W., Liu, Y., Jensen, M.P., Toto, T., Foster, M.J., Long, C.N., 2014. A comparison of multiscale variations of decade-long cloud fractions from six different platforms over the Southern Great Plains in the United States. J. Geophys. Res. Atmos. 119, 3438–3459. doi:10.1002/2013JD019813

Yang, W., Marshak, A., McBride, P.J., Chiu, J.C., Knyazikhin, Y., Schmidt, K.S., Flynn, C., Lewis, E.R., Eloranta, E.W., 2016. Observation of the spectrally invariant properties of clouds in cloudy-to-clear transition zones during the MAGIC field campaign. Atmos. Res. 182, 294–301. doi:10.1016/j.atmosres.2016.08.004

Table 1. Summary of radiation flux analysis results for Girona and Boulder (Table Mountain), year 2014, when using two different thresholds for Max_Diff.

	Girona		Table Mountain	
Max_Diff	100 W m^{-2}	200 W m^{-2}	100 W m^{-2}	180 W m^{-2}
Minutes analyzed	220,658		214,616	
Clear-sky minutes	25,998	36,988	33,813	49,587
Average fractional cloud cover, *fsc*	0.555	0.532	0.560	0.538
Average *fsc* for non-cloudless and non-overcast cases	0.430	0.386	0.441	0.395

Table 2. Average differences between the estimated fractional sky cover ($\Delta\_fsc = fsc\_100 - fsc\_200$) when using the two different Max_Diff thresholds for clear sky identification, only for the non-cloudless and non-overcast cases.

	Girona		Table Mountain	
	Number of minutes	$\langle\Delta\_fsc\rangle$	Number of minutes	$\langle\Delta\_fsc\rangle$
$\Delta\_fsc > 0.05$	35,906	0.11	36,626	0.11
$\Delta\_fsc > 0.10$	15,158	0.16	16,905	0.15
$\Delta\_fsc > 0.20$	2,765	0.29	1,574	0.24
$\Delta\_fsc > 0.30$	757	0.41	106	0.36
Total with $fsc\_200 \leq 0.95$ and $fsc\_100 \geq 0.05$	107,281		102,737	

Table 3. Sensitivity analysis of the cloud screening procedure applied to MFRSR measurements. See Michalsky et al. (2010) for details on the method. Total number of points scrutinized, 208,259 (Girona), 451,793 (Table Mountain).

	Thresholds applied					Number of cases passing the screening	
	Time window (min)	Maximum difference	Maximum range	Maximum relative difference	Maximum relative range	Girona	Table Mountain
Default	10	0.02	0.03	10%	20%	86,701	125,084
1	5	0.02	0.03	10%	20%	103,615	
2	15	0.02	0.03	10%	20%	75,143	
3	10	0.01	0.02	10%	20%	78,604	
4	10	0.03	0.05	10%	20%	90,782	
5	10	0.02	0.03	5%	10%	52,801	
6	10	0.02	0.03	20%	40%	98,146	
Relaxed	5	0.03	0.05	20%	40%	120,221	209,847
Strict	15	0.01	0.02	5%	10%	38,971	37,184

Table 4. Frequency of differences in the thin cloud fraction when two different thresholds are applied in the TSI image processing (instead of the default value of 0.30) for several values of the differences.

Range of differences	Threshold applied	
	0.20	0.40
≤ -0.30	0.0%	1.0%
(-0.30, -0.20]	0.0%	2.8%
(-0.20, -0.10]	0.0%	14.6%
(-0.10, -0.05]	0.0%	29.3%
(-0.05, 0)	0.0%	38.7%
= 0	6.2%	13.6%
(0, 0.05]	36.3%	0.0%
[0.05, 0.10)	35.7%	0.0%
[0.10, 0.20)	16.9%	0.0%
[0.20, 0.30)	4.3%	0.0%
≥ 0.30	0.7%	0.0%

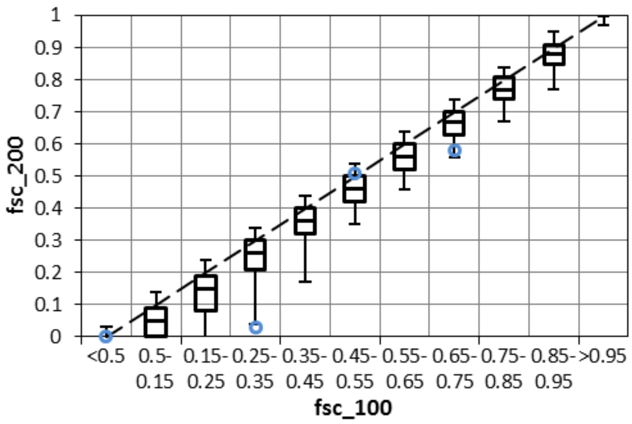

Figure 1. Box-plot of the *fsc* estimated when using Max_Diff = 200 W m^{-2} organized by bins of the *fsc* estimated when using Max_Diff = 100 W m^{-2}. Boxes indicate median and 1st and 3rd quartiles, whiskers indicate percentiles 5 and 95. Data is from Girona. Blue circles indicate the mean values for days presented in Figures 2-5.

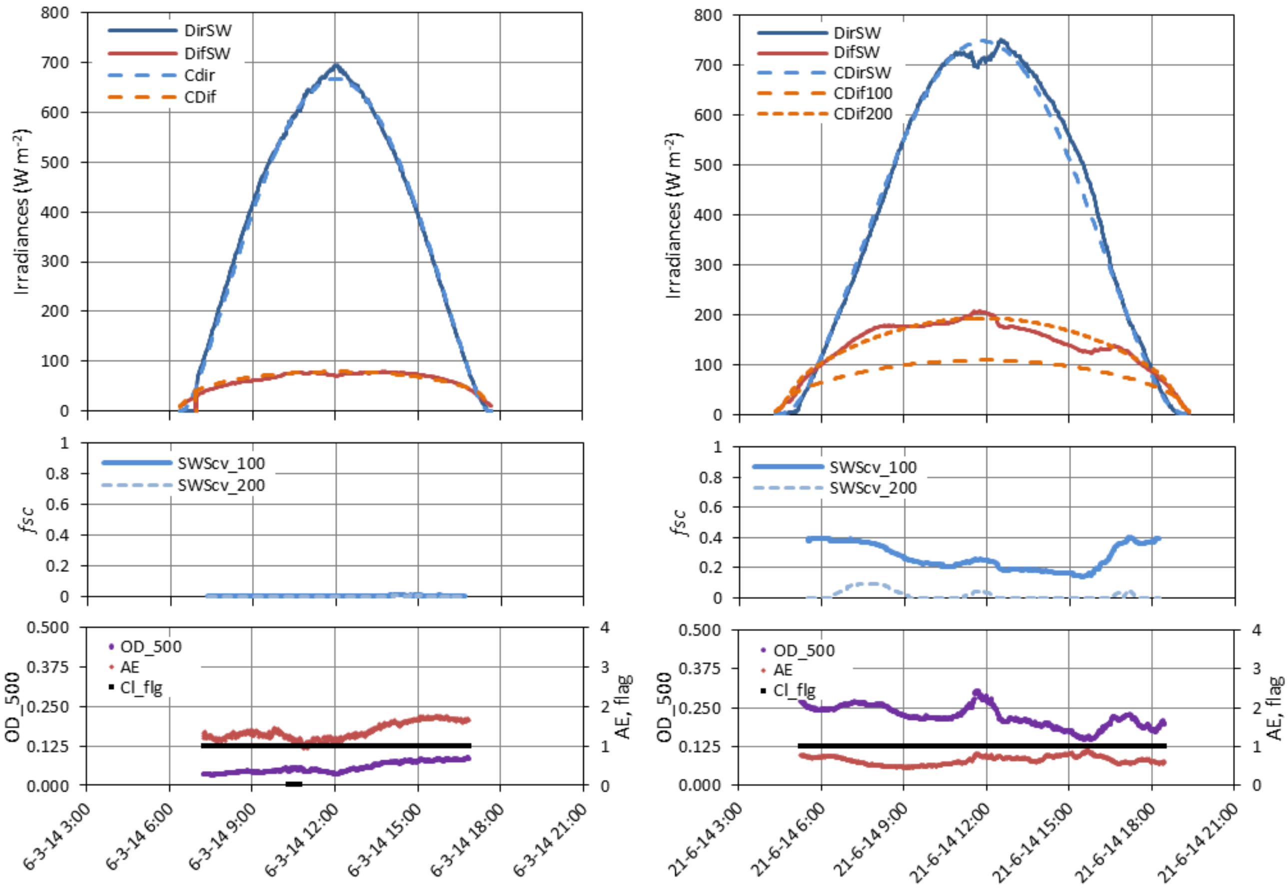

Figure 2. Two examples of “clear” days at Girona. Left, March 6, 2014; right, June 21, 2014. Top panels, diffuse and direct irradiances; middle panels, estimation of fractional sky cover; bottom panels, outputs from the MFRSR: OD, AE, cloud flag.

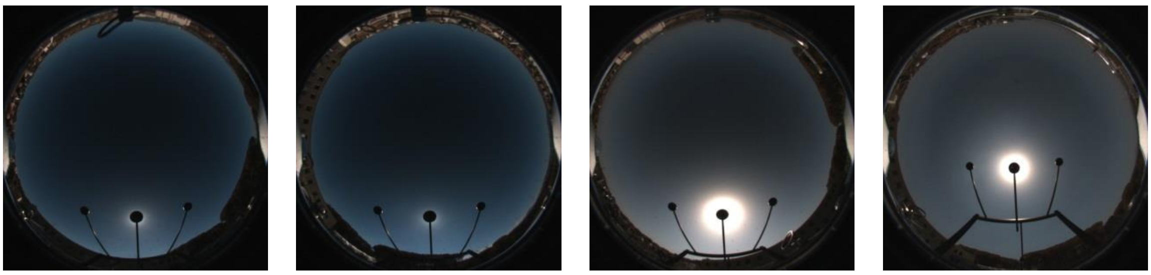

6-3-2014, 10:00 | 6-3-2014, 14:00 | 21-6-2014, 8:00 | 21-6-2014, 14:00

Figure 3. Two sky images for each of the two days represented in Figure 2.

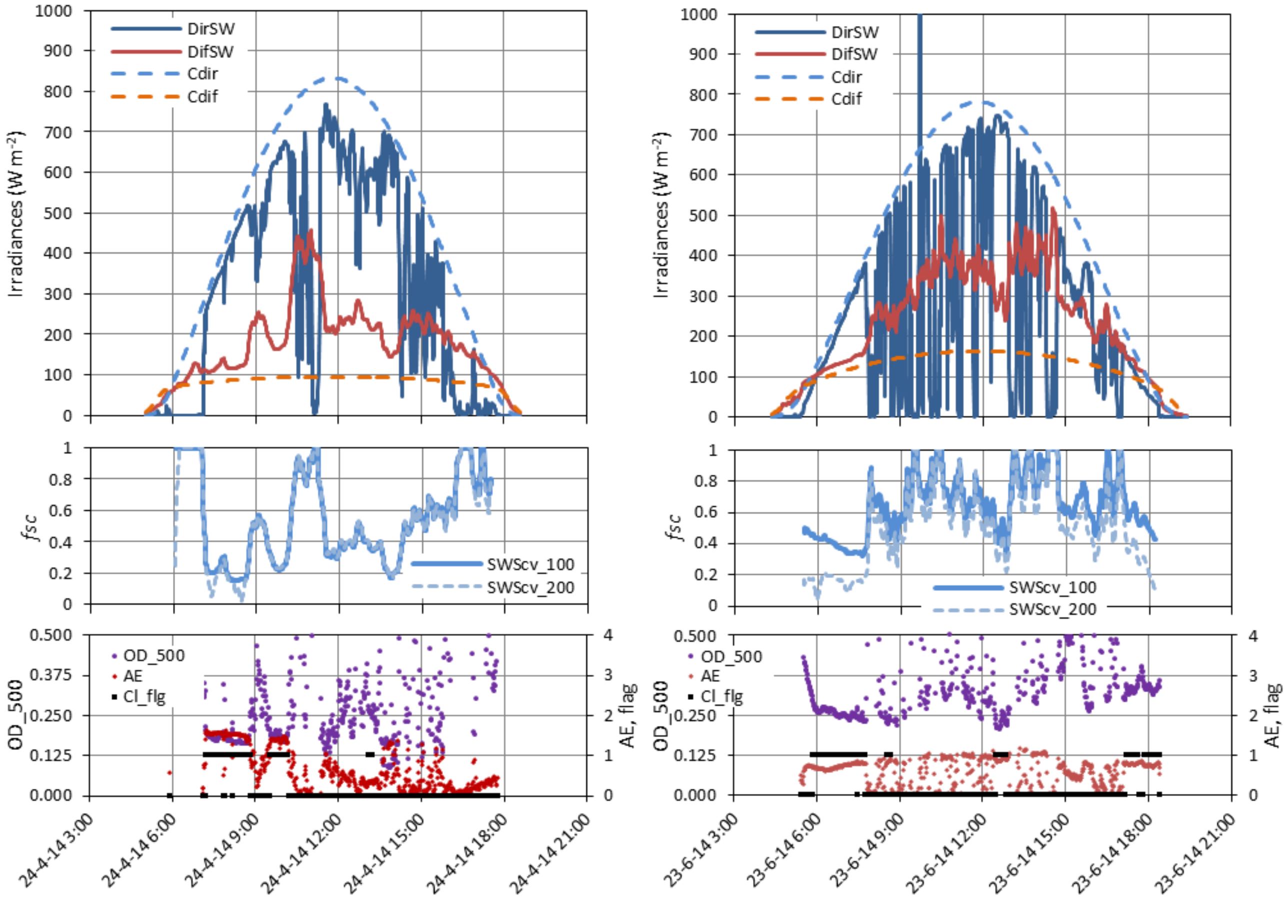

Figure 4. Two examples of variable cloudiness days at Girona. Left, April 24, 2014; right, June 23, 2014. Top panels, diffuse and direct irradiances; middle panels, estimation of fractional sky cover; bottom panels, outputs from the MFRSR: OD, AE, cloud flag.

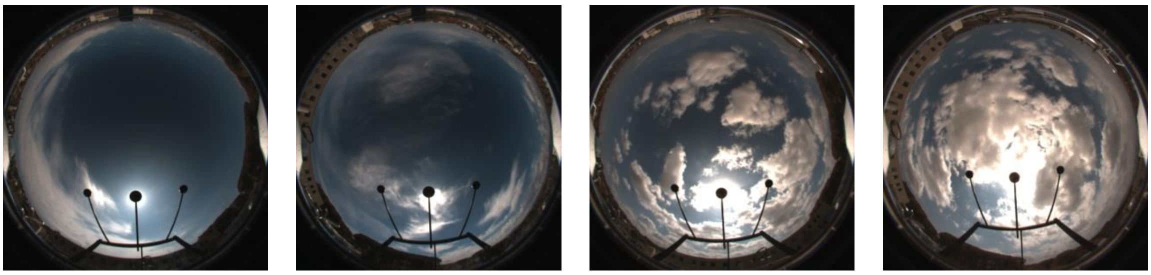

Figure 5. Two sky images for each of the two days represented in Figure 4.

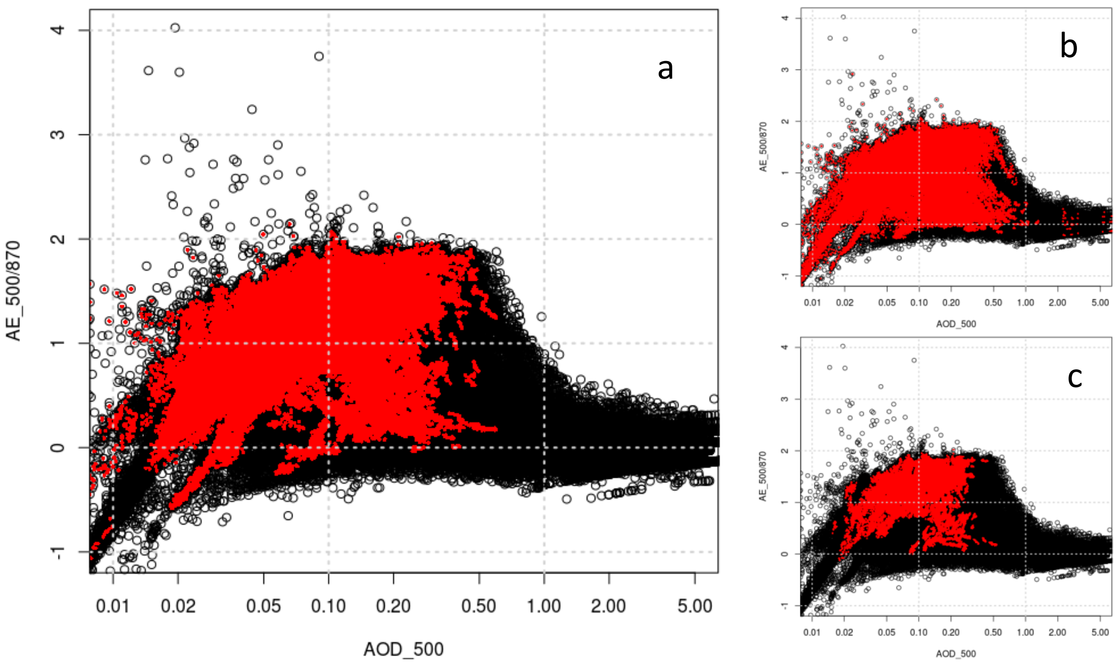

Figure 6. The aerosol Ångström exponent (AE) versus the optical depth (OD) at 500 nm as result of processing the MFRSR spectral measurements of global and diffuse solar radiation. Note the logarithmic scale of the OD axis. Black circles, all data; red dots, data that pass the cloud screening filter. a) Default values in the cloud screening; b) "Relaxed" values; c) More "strict" values. It should be noted that there are points that do not pass the filter which are hidden by the red dots.

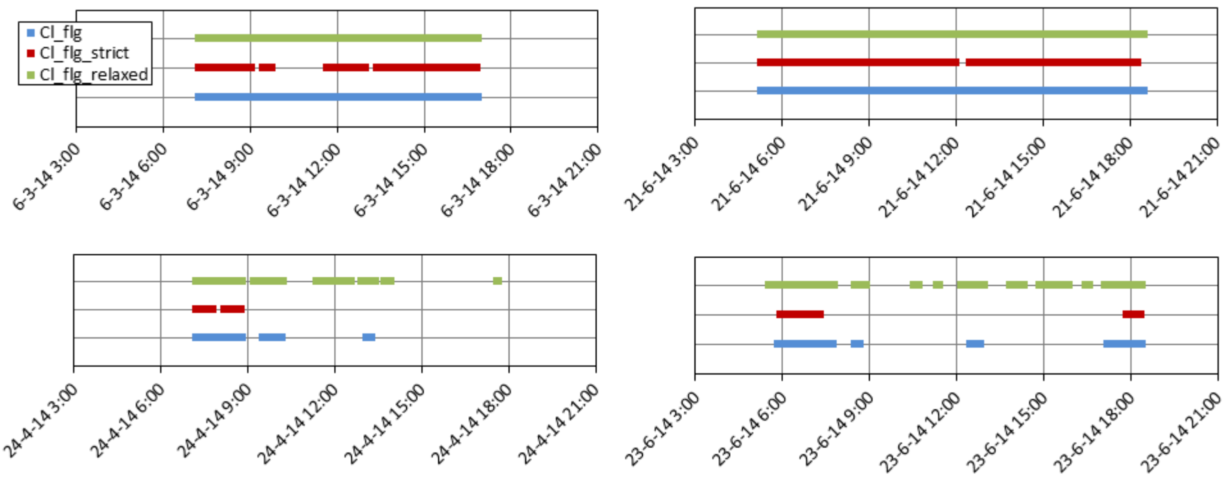

Figure 7. For the four days presented in Figures 1 and 3, periods that are considered “aerosols” by the “default” (blue), “strict” (red), and “relaxed” (green) MFRSR cloud screening.

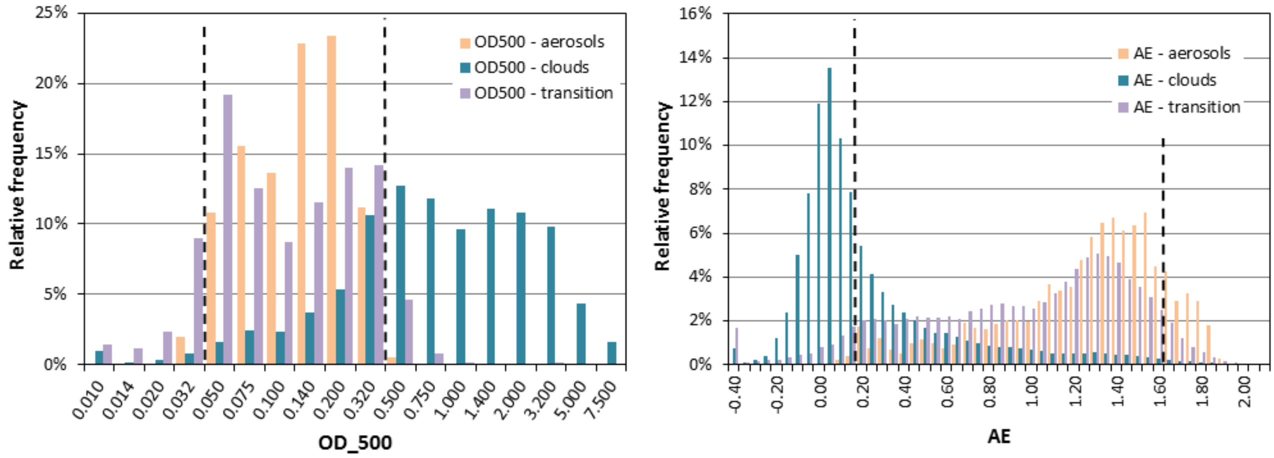

Figure 8. Distribution of the points considered aerosols (38,971 points, orange bars), clouds (88,038 points, blue bars), and "transition" (81,250 points, purple bars) across the range of OD values (left) and AE values (right), after applying the MFRSR cloud screening algorithm with different thresholds. It should be noted that "clouds" refers to instances that have not passed the screening by the MFRSR. Dashed lines indicate the (approximate) percentiles 1 and 99 of the "clouds" and "aerosols" distributions.

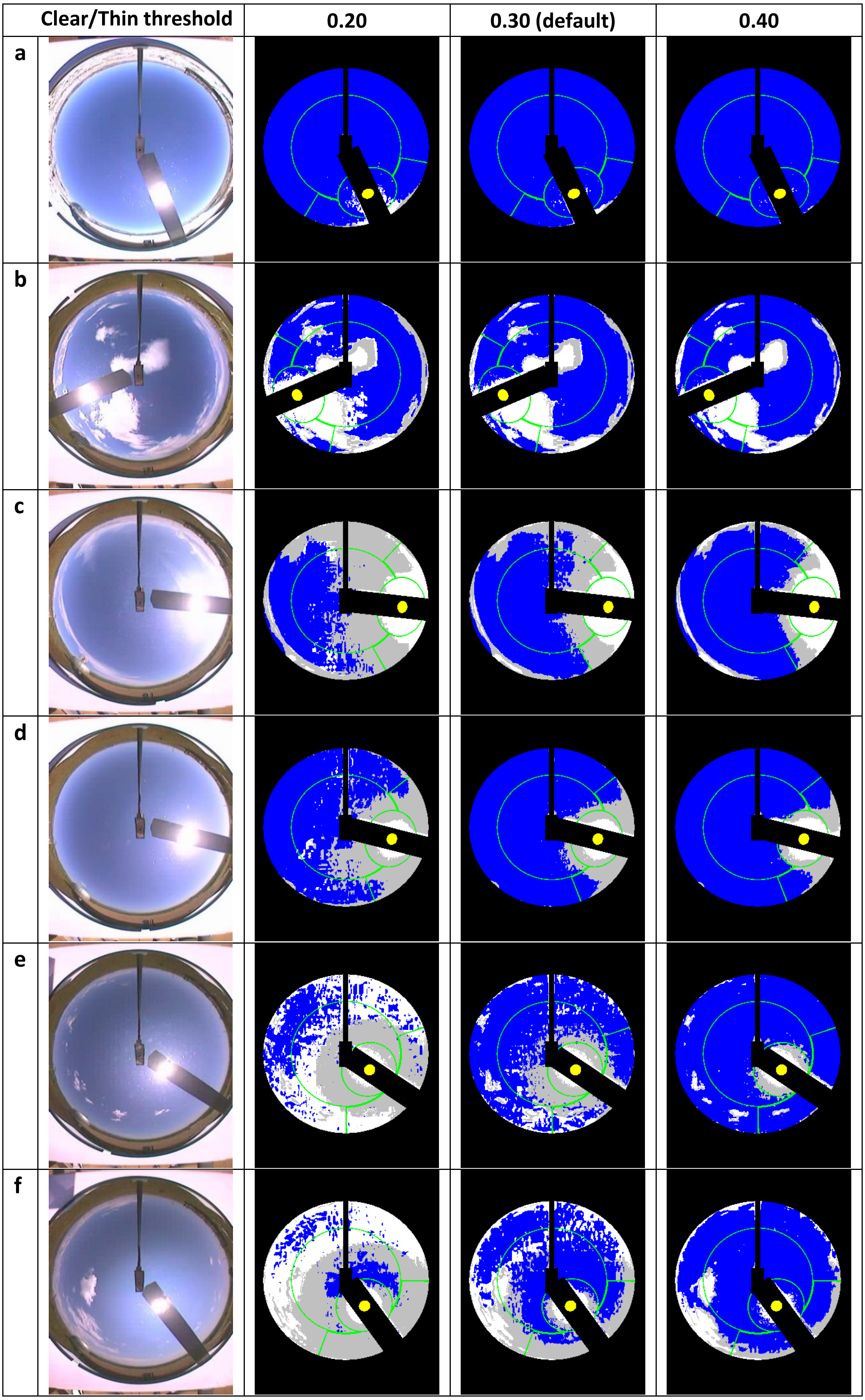
Clear/Thin threshold
0.20
0.30 (default)
0.40
a
b
c
d
e
f

Figure 9. Original and processed TSI images, with different thresholds for the distinction between clear sky and thin clouds. a) March 8, 2014, 11:00. An example of very clean day, when changing the threshold does not affect the cloud fraction estimation. b) August 23, 2014, 15:00. Very white clouds in a very clean (blue) sky. Again, changing the threshold has a very minor effect on the estimation. c) May 16, 2014, 08:14. An example with large circumsolar radiation, where lowering the threshold greatly increases the thin cloud fraction estimation. d) May 19, 2014, 09:00. A similar case, but with an apparently large aerosol load. e) June 10, 2014, 10:30. Small cumulus forming in a somewhat hazy atmosphere. The effect of changing the threshold is huge. f) August 10, 2014, 11:00. A similar case, showing again the large effect of changing the threshold.